

Zweitveröffentlichung/ Secondary Publication



Staats- und
Universitätsbibliothek
Bremen

<https://media.suub.uni-bremen.de>

Schönemann, Lars ; Riemer, Oltmann

Thermo-mechanical tool setting mechanism for ultra-precision milling with multiple cutting edges

Journal Article as: peer-reviewed accepted version (Postprint)

DOI of this document* (secondary publication): <https://doi.org/10.26092/elib/176>

Publication date of this document: 06/09/2024

* for better findability or for reliable citation

Recommended Citation (primary publication/Version of Record) incl. DOI:

Lars Schönemann, Oltmann Riemer,
Thermo-mechanical tool setting mechanism for ultra-precision milling with multiple cutting edges,
Precision Engineering, Volume 55, 2019, Pages 171-178, ISSN 0141-6359,
<https://doi.org/10.1016/j.precisioneng.2018.09.003>.

Please note that the version of this document may differ from the final published version (Version of Record/primary publication) in terms of copy-editing, pagination, publication date and DOI. Please cite the version that you actually used. Before citing, you are also advised to check the publisher's website for any subsequent corrections or retractions (see also <https://retractionwatch.com/>).

This document is made available under a Creative Commons licence.

The license information is available online: <https://creativecommons.org/licenses/by-nc-nd/4.0/>

Take down policy

If you believe that this document or any material on this site infringes copyright, please contact publizieren@suub.uni-bremen.de with full details and we will remove access to the material.

Thermo-mechanical tool setting mechanism for ultra-precision milling with multiple cutting edges

Lars Schönemann^{a,b,*}, Oltmann Riemer^{a,b}

^a Leibniz Institute for Materials Engineering IWT, Department Laboratory for Precision Machining LFM, Badgasteiner Str. 2-3, 28359, Bremen, Germany

^b MAPEX Center for Materials and Processes, University of Bremen, Badgasteiner Str. 1, 28359, Bremen, Germany

ARTICLE INFO

Keywords:

Ultra precision milling
Diamond machining
Tool alignment
Thermo-mechanical actuator
Multi-flute diamond milling

ABSTRACT

Ultra-precision milling operations are particularly ineffective machining processes, due to the fact that they are typically operated with a singular cutting edge (fly-cutting). For meeting the tight tolerances of optical and high precision surfaces, a nanometer precision tool setting mechanism is mandatory when adding more cutting edges. On the basis of a theoretical assessment of the surface generation, this paper presents a novel tool setting mechanism based on a thermo-mechanical actuator that has specific advantages compared to electrical or mechanical solutions. The prototype design for a two-tool holder for diamond milling using this actuator is presented and the choice of substrate material is assessed by FEM simulations. It was found that 1.2083 type steel potentially offers a larger stroke and therefore was chosen for the prototype. Next, the requirements for the heat input are discussed and a novel device for quasi-continuous heating during spindle rotation—an IR-LED ring light—is presented. Using the ring light, it is demonstrated that the tool holder can be selectively heated and a localized expansion of up to $1\ \mu\text{m}$ is achievable at a spindle speed of $240\ \text{min}^{-1}$.

1. Introduction

Ultra-precision milling with diamond tools (Fig. 1) is a fast and flexible way to machine complex surfaces with high demands on surface finish and figure accuracy [1,2]. Although being restricted to a limited spectrum of machinable materials, e.g. Al, NiP, Cu, but not Fe (cf [3]), it is commonly used to directly generate metal mirrors and molding inserts for optical components with freeform [4–6] or micro-structured surfaces [7]. Dutterer et al., for example, used diamond milling to generate freeform infrared optics (“Alvarez lens”) in Germanium [8]. Wu et al. applied trapezoidal diamond tools and a fly-cutting process to machine a mold for a polymer optical waveguide [9]. Fang and Liu used fly-cutting to analyze burr formation in machining of micro-structures [10].

Despite its superior performance in terms of quality, diamond milling is particularly ineffective when it comes to production speed [11]. Brecher et al. calculated the typical surface generation rate of diamond fly-cutting processes to be approximately $2.5\ \text{mm}^2\text{min}^{-1}$ [5]. Hence, the machining of complex optical surfaces can easily require several hours [12] or even days [13] of pure cutting time. In the following, the two main reasons for this ineffectiveness will be described.

Firstly, high speed cutting has been utilized in conventional

machining processes for several decades [14,15], but has not been introduced to ultra-precision machining. This is especially startling since modern air bearing spindles are capable of achieving high speeds of both the workpiece and the tool for several years. In 2012, for example, Precitech machines were equipped with workpiece spindles capable of speeds up to $n = 18000\ \text{min}^{-1}$ and milling spindles capable of reaching $n = 15000\ \text{min}^{-1}$ to $50000\ \text{min}^{-1}$ [16]. Levicron even offers ultra-precision air bearing spindles with a maximum speed $n = 80000\ \text{min}^{-1}$ and more [17,18]. Nevertheless, spindle speeds of $n < 4000\ \text{min}^{-1}$ are still commonly applied in diamond milling [5].

Secondly, ultra-precision milling processes are limited to fly-cutting, i.e. the application of only a singular cutting edge, in order to guarantee a well-defined flycut radius. This is necessary due to the precision of the machined surface which implies characteristic values of $Sa < 10\ \text{nm}$ arithmetic mean height surface roughness and $PV < 0.2\ \mu\text{m}$ peak-to-valley form accuracy [19]. For these values to be met, all factors that influence the surface generation in raster milling have to be considered. If only a single cutting edge is used, the tool nose radius r_f and the swing distance R can be treated as constant and thus may be used to calculate a well-defined surface on the basis of chosen machining parameters. Using a tool holder with multiple tool-inserts, however, leads to different circular paths of the individual cutting edges, due to the

* Corresponding author. Leibniz Institute for Materials Engineering IWT, Department Laboratory for Precision Machining LFM, Badgasteiner Str. 2-3, 28359, Bremen, Germany.

E-mail address: schoenemann@iwt.uni-bremen.de (L. Schönemann).

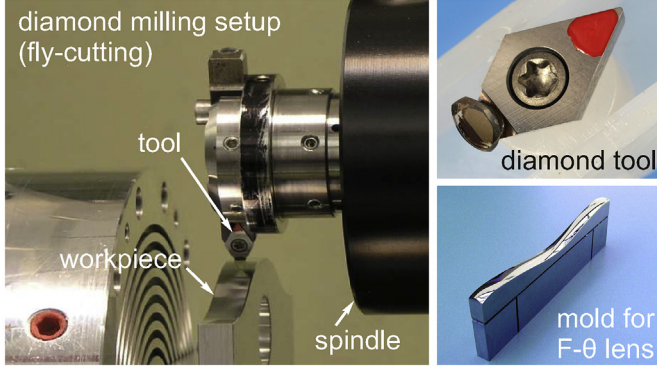


Fig. 1. Diamond milling setup (fly-cutting), diamond tool and milled optical part (mold for f- θ -lens).

tolerances in machining and assembly. Basically, this deviation of the cutting paths causes an increase of the kinematic roughness R_{kin} of the surface up to a point where only the cutting edge of the tool that has the larger flycut radius contributes to the generation of the surface topography. If the deviation is even larger than the maximum chip thickness, the recessed cutting edge is not engaged in the material removal at all.

Both aspects, the low spindle speed and the single cutting edge, are limiting the applicable feedrate v_f , resulting in the aforementioned low efficiency in terms of surface generation or material removal rate. In addition, there is only limited possibility for introducing common automation techniques into the setup procedure, e.g. for referencing the part and the tool or for balancing the spindle. As most procedures have to be conducted manually, extensive setup times are the result.

This paper concentrates on the potential increase of the material removal rate in diamond milling by using tools with multiple cutting edges. First, the theoretical background for calculating the surface roughness in case of multiple cutting edges in diamond machining will be derived in the following section. Then, a novel tool setting actuator will be presented for actively controlling the radial position of a cutting edge and therefore enabling multiple cutting edges on one tool holder.

2. Theoretical considerations

In case of constant fly-cutting radius R and tool nose radius r_ϵ , the kinematic roughness R_{kin} can be calculated from the chosen spindle speed n , the feed f and the step distance s [20]. For the sake of clarity, only the horizontal cutting strategy will be considered in the following calculations, in which f is aligned with the cutting direction and has to be chosen based on R (Equation (1)) and s is orthogonal to the cutting direction and is chosen with respect to r_ϵ (Equation (2)).

$$R_{kin,feed} = R - \frac{1}{2}\sqrt{4R^2 - f^2} \approx \frac{f^2}{8R} \quad (1)$$

$$R_{kin,step} = r_\epsilon - \frac{1}{2}\sqrt{4r_\epsilon^2 - s^2} \approx \frac{s^2}{8r_\epsilon} \quad (2)$$

Now, if more tools are added to the setup, calculating the surface roughness gets more complex, as depicted in Fig. 2. Due to mechanical tolerances of the tool holder, a radial deviation between the respective cutting edges δ unavoidably occurs. For conventional face milling processes with multiple cutting edges, a surface generation model was presented by Franco et al. in Ref. [21]. The model, however, cannot be fully applied here, because it treats all deviations as a shift of the individual cutting inserts. In peripheral milling with horizontal cutting strategy, this is only true in the raster direction, as the tool nose radius is not affected by the setup. In feed direction, however, the deviations results in a change of R . In case of $t = 2$ cutting edges, the resulting surface topography can be approximated by two circles with different

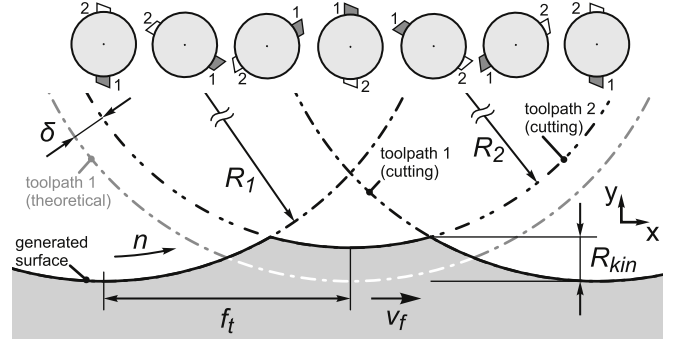


Fig. 2. Surface generation for diamond milling with two cutting edges.

radii R_1 and $R_2 = R_1 - \delta$ whose centerpoints are on the same height $y = R_1$ and have a lateral spacing equal to the applied feed per tooth $\Delta x = f_t$ (see Fig. 2 and Equations (3)–(6)).

$$x_1 = R_1 \cos(t) \quad (3)$$

$$y_1 = R_1 \sin(t) + R_1 \quad (4)$$

$$x_2 = R_2 \cos(t) + f_t = (R_1 - \delta)\cos(t) + f_t \quad (5)$$

$$y_2 = R_2 \sin(t) + R_1 = (R_1 - \delta)\sin(t) + R_1 \quad (6)$$

with $(0 \leq t \leq 2\pi)$

By determining the intersection points $(x_1 = x_2 \wedge y_1 = y_2)$ between these two circles, the resulting kinematic surface roughness can be calculated.

$$x_i = \frac{f_t^2 + 2\delta R_1 - \delta^2}{2f_t} \quad (7)$$

$$y_i = R_1 - \sqrt{R_1^2 - x_i^2} = R_{kin,2} \quad (8)$$

$$R_{kin,2} \approx \frac{(f_t^2 + 2\delta R_1 - \delta^2)^2}{8f_t^2 R_1} \quad (9)$$

In reality, the rotation of the milling tool is superimposed by the feed motion. Therefore, the cutting edges do not move on an exactly circular, but on a trochoidal tool path. To check whether the approximate calculations made here are valid, they were compared to the surface roughness generated by a trochoidal tool movement (Equations (10)–(13), cf [19]).

$$x_{t1} = v_f t + R_1 \sin(\omega t) \quad (10)$$

$$y_{t1} = R_1 - R_1 \cos(\omega t) \quad (11)$$

$$x_{t2} = v_f t + R_1 \sin(\omega t + \pi) \quad (12)$$

$$y_{t2} = R_1 - (R_1 - \delta)\cos(\omega t + \pi) \quad (13)$$

with $\omega = 2\pi n$ and $v_f = f_t n$

In contrast to the example of Cheng et al., calculating a closed form solution for the intersection of the trochoids is not trivial. Hence, the intersection was calculated numerically. For typical values, e.g. $R_1 = 23$ mm, $f_t = 15$ μ m and $\delta = 4$ nm, the calculated kinematic roughness using the circle method is $R_{kin,2c} = 4.0406$ nm compared to $R_{kin,2t} = 4.0404$ nm using the trochoidal method. For smaller R_1 , larger f_t and larger δ , the relative difference increases (Fig. 3). Nevertheless, as long as $R_1 \gg f_t$, it remains $< 1\%$. Thus, it can safely be assumed that the calculations on the basis of circular movements is sufficiently accurate under these conditions.

On the basis of the assumptions for calculating the surface generation in feed direction, some conclusions for diamond milling with multiple cutting edges may be derived:

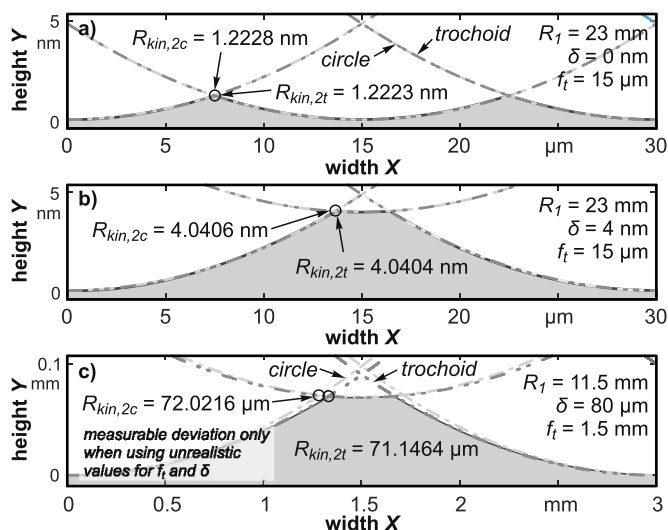


Fig. 3. Modeled surface topography for selected parameters and calculated kinematic roughness with circle and trochoid-based approximation. N.B. Third set of parameters demonstrates model deviation at extreme values that are typically not viable for diamond milling.

1. A radial deviation δ of the cutting edges always leads to an increase in surface roughness. For maintaining the desired kinematic roughness R_{kin} , the feed velocity $v_f = n f_t$ has to be decreased from the maximum theoretical value with respect to δ (i.e. solve Equation (9) for f_t). This, however, reduces the efficiency of the process.
2. If the deviation of the cutting edges δ is larger than kinematic roughness generated by only the outer tool (i.e. $R_{kin,1} = \frac{1}{2} f_t^2 R^{-1}$ for $t = 2$), the inner tool is not engaged in the surface generation, but does remove a proportion of the workpiece material.
3. When the deviation increases above the maximum chip thickness of the outer tool, the inner tool is not engaged in the material removal at all.

Thus, to effectively utilize more than one cutting edge in a diamond milling process, an alignment mechanism for correcting the radial position of the tools is mandatory. The underlying actuator must achieve a maximum stroke large enough to compensate typical misalignment from the manual tool setup. The precision of the actuator has to be at least better than the maximum chip thickness for the second tool to contribute to the material removal. If the precision is better than the kinematic roughness generated by applying only one tool with the given set of process parameters, the feedrate may be accelerated accordingly, resulting in an increased material removal rate and thereby a more economic process. Additional adjustable tools will further increase the efficiency.

3. Thermo-mechanical tool setting mechanism

The required tool setting accuracy of a few nanometers cannot be achieved solely by mechanical means, e.g. slide mechanisms or micrometer threaded screws. Piezoelectric actuators, for example, are capable of achieving a (sub) nanometer precision, but also require an electrical power supply and a feedback signal, which, in case of milling operations, has to be provided on the rotor of the spindle carrying the tool holder. Using a slip ring for power supply and data transfer directly affects the runout of the air bearing spindle and thus influences the generated surface topography, see Ref. [22]. Another option would be to integrate a power supply and a micro controller onto the spindle rotor. This, however, increases mass and volume of the rotor and results in a poor dynamic behavior of the spindle.

In this context, the application of a thermo-mechanical actuating

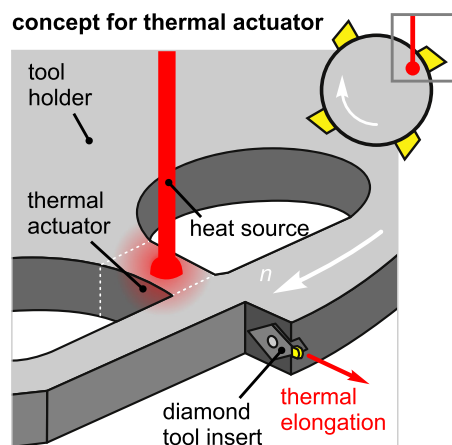


Fig. 4. Concept for a thermal actuator for precision tool setting in diamond milling, cf [23].

mechanism is seen as a suitable approach (Fig. 4). Here, the tool holder itself is heated up locally, resulting in a thermal elongation of the substrate material. This concept has, potentially, several advantages, but also challenges that have to be counteracted:

- The required heat input may be transferred contactless, e.g. by using infrared radiation or induction heating, and therefore does not influence the dynamic behavior of the spindle and does not introduce additional disturbances to the milling process.
- Thermal processes are generally elapsing slowly and thus, a previously set elongation can be maintained with a minimum input of heat and thus kept constant over a long time.
- With known physical properties of the tool holder substrate, the required heat input may be calculated on the basis of a mathematical model and thus be used in the closed loop control of the elongation.
- Undesired heat input has an impact on the thermal state of the machine tool and thus should be avoided or reduced to a minimum. In the present case, as only a small heat input is necessary to expand e.g. a steel substrate by several nanometers, the overall thermal stability of the machine tool should not be affected.
- Coolant and forced convection will influence the thermal state of the tool holder and thus affect the long-term stability of the expansion. Therefore, the systems needs to be capsuled for use in a machining environment.

In this case, infrared radiation was chosen as heat generator. Preliminary results on the design of the actuator have been subject of previous publications, concentrating on the initial design of the actuator used in a static test stand [24], its evaluation concerning surface properties and environmental conditions [25] as well as the establishment of a closed loop control [23]. It has been shown that a stroke of >1000 nm may be achieved with this setup, even under forced convection. By using a closed loop control, a precision of <10 nm is achieved. On the basis of these findings, a new actuator design for the application on a spindle setup will be outlined here.

3.1. Tool holder design for spindle setup

For validating the concept of thermo-mechanical tool alignment in a rotating environment, the actuator has to be integrated into a tool holder for diamond milling. The actuator itself is basically a bar type element with a width of 20 mm, a length of 25 mm and a thickness of 12 mm that is placed near the outside diameter of a 130 mm tool holder. The size of the steel disc allows for up to four thermal actuators to be integrated. However, the current design only features two at 180°

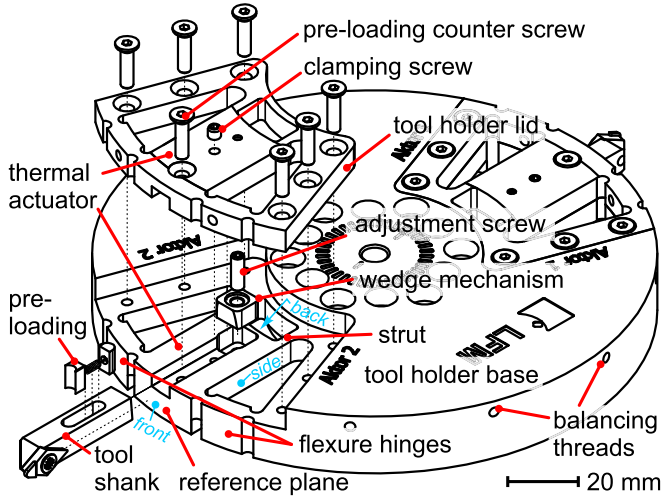


Fig. 5. Design of adjustable tool holder for diamond milling with two cutting inserts.

spacing for reasons of symmetry and simplicity (Fig. 5).

The side of the actuator is cut free in order to allow for an undisturbed expansion of the actuator and minimal heat transfer to the substrate. Thus, the back of the actuator is attached to the tool holder by two 2.5 mm wide struts, while its front face is connected via two flexure hinges. The latter allow for a radial displacement but provide additional stiffness in the tangential (i.e. cutting) direction. Furthermore, the actuator is placed slightly asymmetric to the vertical midplane of the tool holder, so that the rake face of the diamond tool insert coincides with the midplane.

For pre-alignment of the diamond tool in radial direction, the actuator features an internal mechanical mechanism. For its integration, the actuator is sliced horizontally to obtain a basis (i.e. the tool holder) and a removable lid, both of which feature a groove that can accommodate a tool shank of 6.35 mm square cross section. The rear face of the tool shank is ground at an angle of 5° and pre-loaded against a movable wedge with the same angle. By moving the wedge via a precision set screw, the tool shank is precisely shifted in the radial direction. Preliminary experiments using a similar mechanism in a static test stand have shown, that a tool setting precision of better than $1 \mu\text{m}$ is achieved in this way, so that the remaining deviation can be compensated by the thermal actuator itself. After the pre-alignment is completed, the tool shank is clamped by two set screws. An additional screw acts as the counterpart for the pre-loading and prevents the tool shank from accidentally being released from the mechanism at high spindle speeds.

Compared to the static test setup, based on 1.7225 type steel, the tool holder for the spindle is made of 1.2083 type steel. This alloy features a lower thermal conductivity ($\kappa_{2083} = 22.6 \text{ W m}^{-1} \text{ K}^{-1}$ vs. $\kappa_{7225} = 42.6 \text{ W m}^{-1} \text{ K}^{-1}$) and the same coefficient of thermal expansion ($\alpha = 11.1 \mu\text{m m}^{-1} \text{ K}^{-1}$). Thus, it achieves a similar stroke at a longer time constant, which was predicted by preliminary finite element (FE) simulations (Fig. 6).

For this, a STEP model of the actuator design was imported into a commercially available FE-software (Autodesk Simulation Mechanical 2016) and meshed accordingly. As boundary condition, a natural convection of all faces to room temperature (20°C) was added and a load resembling two LED light sources was introduced at the same position on the top and bottom face of the actuator. Therefore, the radiant intensity of the LED was converted into a load that is directly applied to the finite elements, assuming an absorption coefficient of $\eta = 40\%$. Then, the transient heat transfer was calculated according to the material properties of the selected steel types. In a second step these results were used as load for the calculation of the thermally induced static

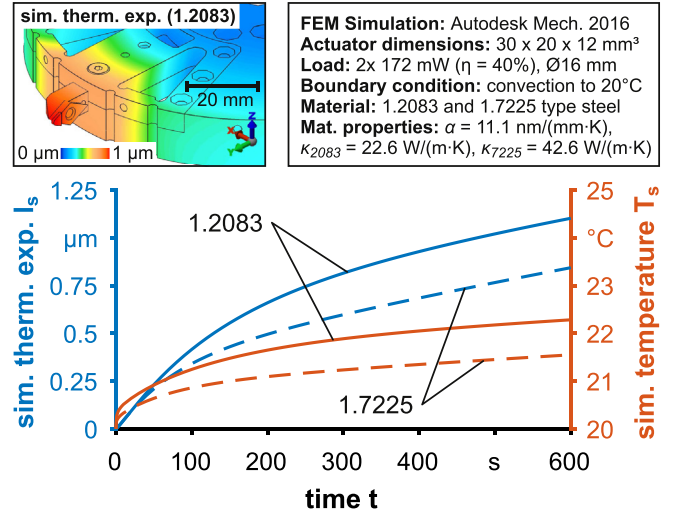


Fig. 6. FE-simulation of the thermal expansion for 1.2083 and 1.7225 type steel.

stresses. Fig. 6 shows the resulting temperature of a single point on the top face and the shift of the tool tip as a result of the thermal expansion for both steel types.

It can be seen that after $t = 600 \text{ s}$ of constant heat input, the 1.2083 type steel is able to reach a significantly higher temperature of $T_{\text{max},2083} = 22.29^\circ\text{C}$ than the 1.7225 alloy ($T_{\text{max},7225} = 21.55^\circ\text{C}$) and features improved corrosion resistance. This results in a larger thermal expansion of the stainless steel actuator ($l_{\text{max},2083} = 1103 \text{ nm}$) than of the 1.7225 ($l_{\text{max},2083} = 844 \text{ nm}$). Thus the 1.2083 type steel is favorable for the novel tool holder design.

3.2. Intermittent control of heat input using a ring-light system

The performance of the actuator ultimately has to be evaluated under rotation. This requires a triggering of the heat source to only illuminate the desired proportion of the tool holder, i.e. only one of the actuators or each actuator with a dedicated heat input. However, if only a single LED is used as a heat source, the illumination time per revolution is severely limited to only a few micro-to milliseconds. In general, the pulse duration t_p of the LED has to be set according to the applied spindle speed and the actuator width (arc length). For example, illuminating a $b = 20 \text{ mm}$ wide actuator on a diameter of $d = 100 \text{ mm}$ (i.e. $\approx 20/300$ of the circumference), a pulse width of about 4 ms is necessary at a typical spindle speed of $n = 1000 \text{ min}^{-1}$. Increasing the spindle speed to the HPC domain (20000 min^{-1}), however, reduces the timespan to only $200 \mu\text{s}$. First evaluations using a static test stand have shown that in this context, a single LED is not sufficient for a stable heating of the substrate, as the actuator cools down quickly during rotation.

A novel approach for heating the rotating tool holder is the use of a ring light system (Fig. 7, top). This stationary device contains multiple of the required IR-LED on the appropriate diameter. To follow the rotation of the tool holder, the individual LED have to be switched on an off according to the angular position of the target segment. As the LED themselves are cheap components, this solution is far more economic (and safe) than using a high power IR heat source, such as a laser diode.

According to the example above, the respective LED needs to be switched on for $200 \mu\text{s}$ to 4 ms , depending on the given spindle speed. As the LED have rise and fall times of 11 ns and 14 ns respectively, the maximum power is emitted almost instantaneously. For emitting their maximum power of 2300 mWsr^{-1} , the utilized IR-LED require an electrical current of $I_F = 1 \text{ A}$ to 2 A at a forward voltage of $V_F = 1.65 \text{ V}$ to 1.9 V . In the present case, this is provided by a standard LED controller

LED ring light

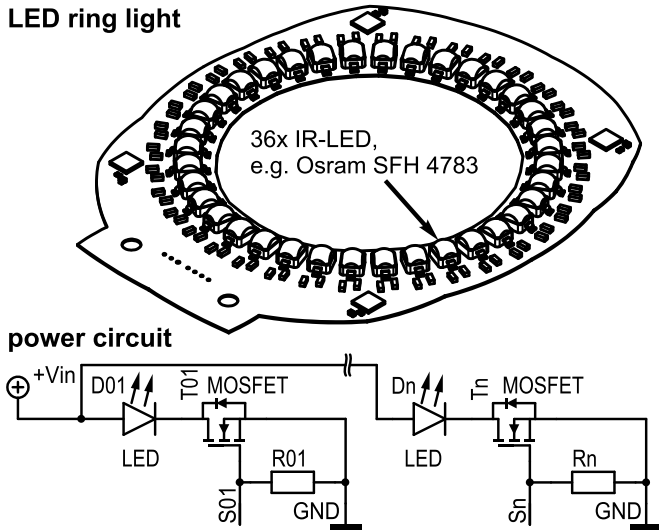


Fig. 7. Sketch of the ring light with 36 identical IR-LED (top) and power circuit using MOSFETs (bottom).

as a common supply voltage $+V_{in}$. By using individual switches, such as metal-oxide semiconductor field-effect transistors (MOSFETs), a connection between $+V_{in}$ and GND is established and a specific LED can be activated, requiring only a small switch signal S_x . The wiring of such a power distribution circuit is shown in Fig. 7 (bottom).

For synchronizing the rotation of the tool holder and the ring light, another electronic circuit was designed that provides the correct sequence of switch signals according to the angular position of the spindle. Both the design of the ring light and its control electronics have been applied for patent and thus will not be discussed further in this context. The patent (reg. no. DE 10 2017 119 828.8) is due for publication in the first quarter of 2019.

4. Evaluation of thermal actuator on spindle setup

In the following sections, the performance of the mechanical pre-alignment mechanism and the thermal actuator are presented and discussed. For all tests, the actuator was mounted on a motorized Professional Instruments Model 4R BlockHead[®] air bearing spindle. The setup is shown in Fig. 8.

The required heat input is generated by two ring lights using 36 Osram SFH-4783 infrared LED each. The LED feature a centroid wavelength of $\lambda_c = 850$ nm, a half angle of $\varphi = \pm 12^\circ$ and a radiant intensity of $I_e = 2.3$ Wsr⁻¹. The thermal expansion is measured at the reference ring via a capacitive sensor (CPL-490 with 2G-C8-0.5 probe from IBS Precision Engineering) that has a resolution of 1 nm at a bandwidth of 50 kHz, across a 50 μ m measuring range. The performance of the pre-alignment mechanism is assessed via a dial gauge.

4.1. Pre-alignment mechanism

The results for the pre-alignment mechanism are shown in Fig. 9. The two point clouds show the measured shift l of the tool shank in outwards and inwards direction, i.e. for increasing and decreasing the fly-cut radius, against the revolution of the fine threaded adjustment screw in 90° increments. In addition, a linear fit of both measurements is shown in Fig. 9.

The inward and outward motion exhibits a small hysteresis, which is due to the missing pre-loading of the shank in this case. The maximum measured shift is $l_{max} = 181$ μ m, which is close to the theoretical maximum of $l_{th} = 11$ rev \cdot 0.2 mm/rev \cdot tan5° = 192.48 μ m. The shift per revolution of the set screw was determined via the fit to be $\Delta l_{rev} = 16.94$ μ m which also is near the theoretical value of

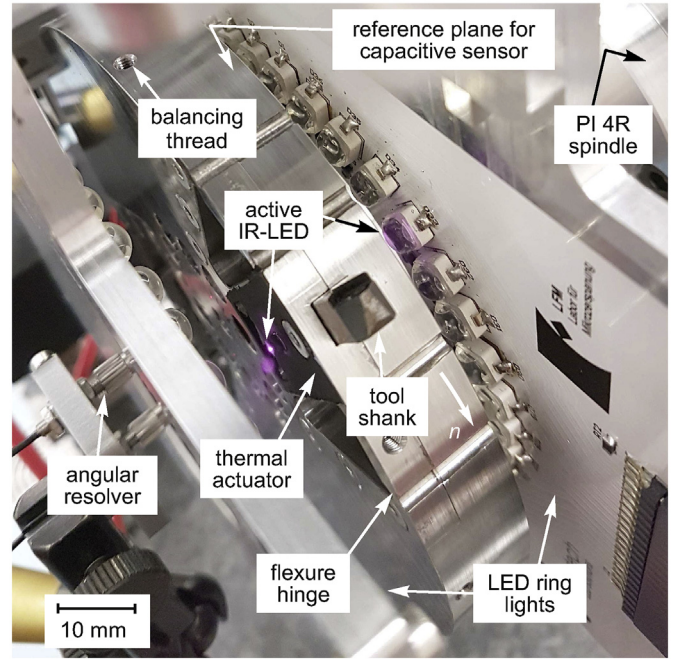


Fig. 8. Test setup on Professional Instruments Model 4R spindle.

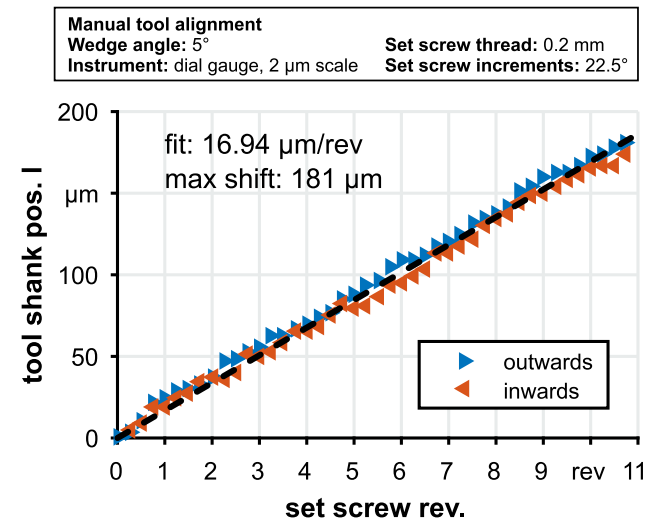


Fig. 9. Radial shift of tool shank via wedge mechanism.

$\Delta l_{rev,th} = 17.5$ μ m. The remaining deviations are attributed to machining and assembly tolerances of the tool holder. This means that a 1/17 revolution (21.18°) of the set screw has to be performed in order to achieve the desired accuracy of $\Delta l_{des} < 1$ μ m. Previous experiments have already shown that smaller increments might be set manually.

4.2. Thermal expansion (clamped spindle)

The thermal expansion of the novel actuator was first evaluated with a clamped spindle, in order to compare its performance with the static setup and the FE-simulations. Both LED light rings were mounted with a distance of 10 mm to the front and the back face of the tool holder, respectively. For assessment of the static actuator performance, a single LED of the light ring was continuously operated at full power and the position of the reference plane was measured using the capacitive probe, until a saturation could be observed. Each measurement was repeated three times in order to analyze the repeatability Fig. 10.

Thermal expansion: Actuator (1.2083 type steel) on PI Model 4R
Heat source: Osram SFH-4783, $\lambda_c = 850 \text{ nm}$, $\phi = \pm 12^\circ$, $l_e = 2.3 \text{ W/sr}$
Metrology: IBS CPL 490, 2G-C8-0.5, $f = 100 \text{ Hz}$

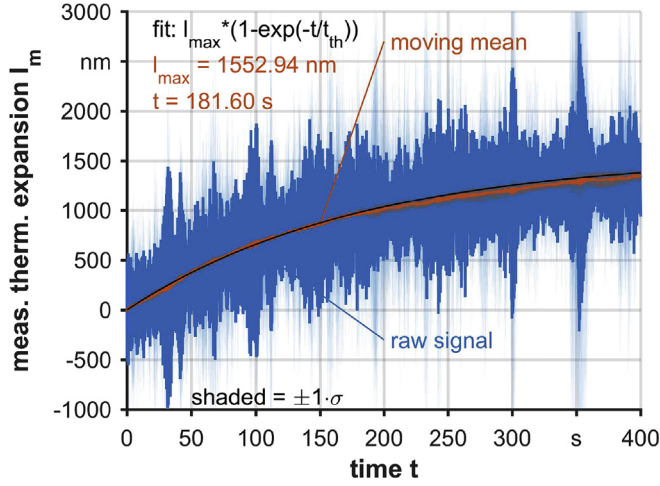


Fig. 10. Measured thermal expansion of the 1.2083 based actuator on the PI Model 4R spindle.

The measurement shows a large noise in the raw signal (blue) which was later attributed to a coupling system that deliberately reduces the stiffness of the spindle mount in radial direction in order to facilitate ultra-precision balancing procedures, see Ref. [26]. In the present case, with a clamped spindle and therefore non-moving actuator, this system only amplifies the measurement noise, but does not affect the amplitude of the thermal expansion. Thus, a moving mean function across 100 values was applied to obtain a stable signal for the static actuator performance (red). Then, an exponential function (Equation (14)) was fitted to the measured data to obtain characteristic values for the maximum thermal expansion l_{max} and the time constant t_{th} .

$$l_m(t) = l_{max} \cdot (1 - e^{-t/t_{th}}) \quad (14)$$

The calculated expansion of $l_{max} = 1553 \text{ nm}$ and time constant of $t_{th} = 181.6 \text{ s}$ for this measurement exceed the expectations derived from the FE-simulations (Fig. 6). As the maximum thermal expansion exceeds 1000 nm, it is deemed sufficient for the intended purpose of compensating the remaining deviation after manual tool setting. Furthermore, the long time constant is expected to facilitate a control of the actuator to reach and hold a defined position.

4.3. Performance under rotation

For a first assessment of the actuator performance under rotation, heating by the LED and measurement of the reference plane were done continuously while rotating the spindle at a specific frequency. Here, it was ensured that the coupling system was clamped in order to reduce measurement noise. The raw measurements are shown in Fig. 11 showing several consecutive revolutions of the spindle at $n = 300 \text{ min}^{-1}$.

The signal shows additional disturbances during rotation, comprising the runout of the reference plane as well as the unbalance of the tool holder and other spindle dynamics. Nevertheless, a repeating (sinusoidal) pattern can be observed. The measured signal gets out of range on several occasions during one revolution, which is due to the cutouts of the flexure hinges. After processing the signal and isolating a single revolution, it was found that although the bandwidth of the measurement was at a very high rate of $f = 10000 \text{ Hz}$, only very few data points are obtainable for the position of the actuator. For a reliable assessment of the thermal expansion, either the measurement rate has to be increased further or the signal has to be averaged over several

Spindle setup: PI Model 4R, $n = 240 \text{ min}^{-1}$
Heat source: Osram SFH-4783, $\lambda_c = 850 \text{ nm}$, $\phi = \pm 12^\circ$, $l_e = 2.3 \text{ W/sr}$
Metrology: IBS CPL 490, 2G-C8-0.5, $f = 10000 \text{ Hz}$

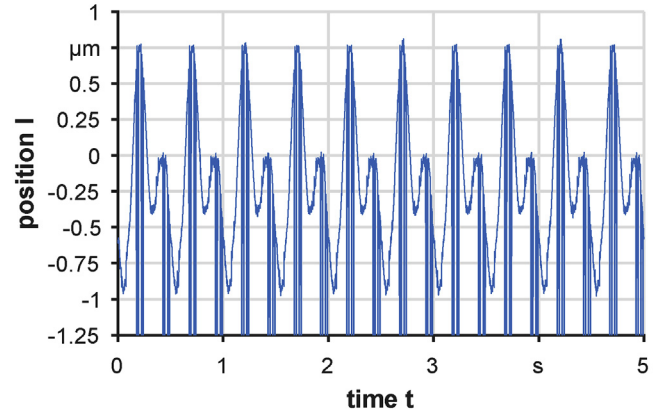


Fig. 11. Measurement of the reference plane with rotating spindle: raw data of 10 consecutive revolutions.

revolutions.

Nevertheless, the signal has to be processed for evaluating the performance of the actuator. This was done using a Matlab script that first splits the raw data according to the spindle frequency into segments of equal duration. Each segment then contains the measurement of one revolution. For further evaluation, the signal dropouts are analyzed, whereas each dropout stands for the beginning of a new section.

In Fig. 12, it can be seen that eight sections of three different types can be identified for one revolution:

- two sections (actuator 1 and 2) with the measurements for the actuators; here, the thermal expansion should be visible
- four sections (flexure 1–4) containing the measurement of the flexure hinges, one before and one after each actuator segment; these should slightly shift according to the thermal expansion
- two sections (reference 1 and 2) containing the measurements of the reference plane of the tool holder body; this takes up the largest proportion of the measurement and ideally should not change

Spindle setup: PI Model 4R, $n = 240 \text{ min}^{-1}$
Heat source: Osram SFH-4783, $\lambda_c = 850 \text{ nm}$, $\phi = \pm 12^\circ$, $l_e = 2.3 \text{ W/sr}$
Metrology: IBS CPL 490, 2G-C8-0.5, $f = 10000 \text{ Hz}$

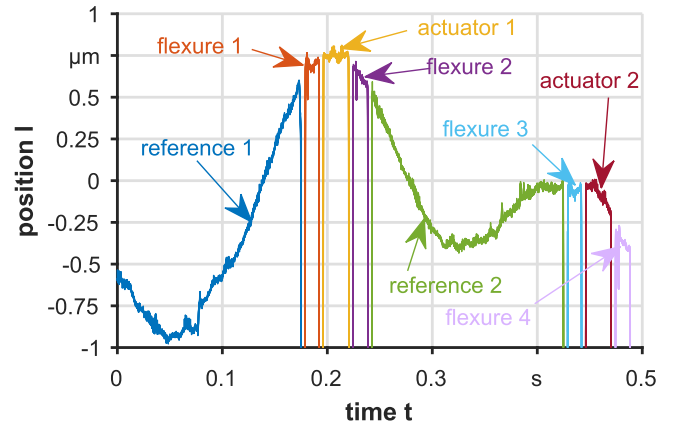


Fig. 12. Measurement of the reference plane with rotating spindle: segmentation of a single revolution and association of segments to actuator geometry. Please note that the last signal dropout is not completely shown and thus the curve does not start and end at the same position.

Spindle setup: PI Model 4R, $n = 240 \text{ min}^{-1}$
Heat source: Osram SFH-4783, $\lambda_c = 850 \text{ nm}$, $\phi = \pm 12^\circ$, $l_e = 2.3 \text{ W/sr}$
Metrology: IBS CPL 490, 2G-C8-0.5, $f = 10000 \text{ Hz}$

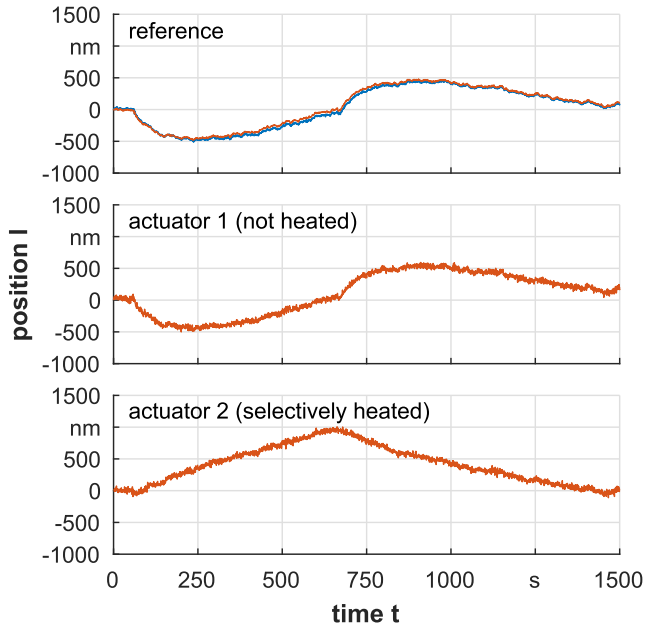


Fig. 13. Temporal development of the measured location of the two reference planes (two curves in top graph), actuator 1 (middle graph) and actuator 2 (bottom graph) while selectively heating a single actuator segment (actuator 2). Each datapoint shows the mean value of the measured segment at the respective time interval after subtracting the runout of the spindle, i.e. the mean of the first 10 revolutions.

during the measurements

After segmentation, each segment is filtered using a first order low-pass filter (Butterworth) with a cutoff-frequency of $\lambda_c = 100 \text{ Hz}$ to reduce the remaining measurement noise. For evaluating the temporal development of the actuator expansion, the first ten segments of the sequence (i.e. the first 10 revolutions of the spindle) are taken as reference for removing the systematic deviations (runout, unbalance etc.) of the measurements. After removing these deviations, the mean value of each segment is calculated and saved along with the starting time of the segment. Fig. 13 shows the temporal development of the reference planes and the two actuator segments, i.e. the mean values of the segments at their associated times.

It can be seen, that a significant difference exists between actuator 1, that is not heated, and actuator 2, that is selectively heated by the IR-LED. However, a systematic deviation still is present in the measurements, as can be deduced from the development of the reference planes which seem to move in the opposite direction of the thermal expansion. It is assumed that this occurs either due to long-term drift of the measured signal or improper filtering/referencing. However, further experiments are necessary to verify the actual cause of this deviation. Nevertheless, after removing this trend from all measurements, i.e. subtracting the mean of both reference curves, the typical exponential trend of thermal expansion is visible (Fig. 14). Overall, a total expansion of $1 \mu\text{m}$ was measured for actuator 2 after 600 s of IR irradiation at $n = 240 \text{ min}^{-1}$. Actuator 1 on the other hand showed no significant expansion. This confirms the feasibility of the proposed approach for using a selective thermal expansion for tool setting in a diamond milling process.

With respect to the required accuracy discussed in section 2 of this paper, it now has to be verified if the thermal expansion can be controlled at level of precision, i.e. with sub-10 nm setpoint accuracy. For

Spindle setup: PI Model 4R, $n = 240 \text{ min}^{-1}$
Heat source: Osram SFH-4783, $\lambda_c = 850 \text{ nm}$, $\phi = \pm 12^\circ$, $l_e = 2.3 \text{ W/sr}$
Metrology: IBS CPL 490, 2G-C8-0.5, $f = 10000 \text{ Hz}$

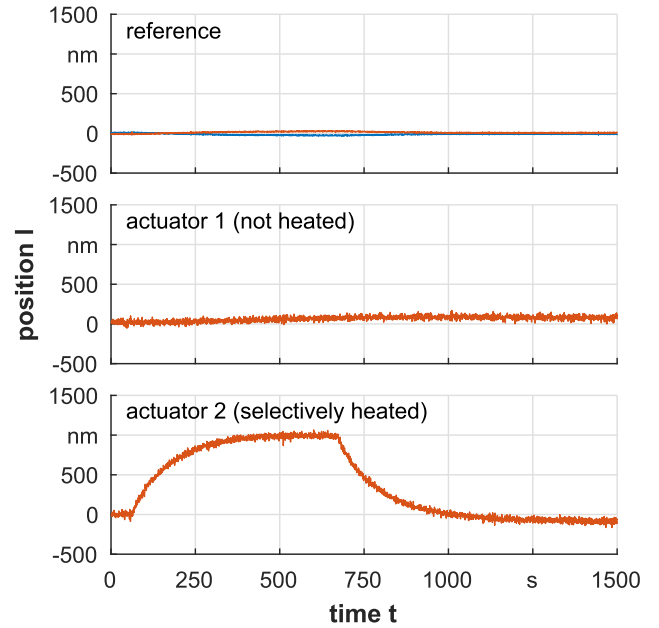


Fig. 14. Temporal development of the measured location of the two reference planes (two curves in top graph), actuator 1 (middle graph) and actuator 2 (bottom graph) while selectively heating a single actuator segment (actuator 2). Each datapoint shows the mean value of the measured segment at the respective time interval after subtracting the runout of the spindle (i.e. the mean of the first 10 revolutions) and the trend of the reference planes (i.e. the mean of both curves in the reference graph) as an additional systematic deviation.

the setup with non-rotating spindle, a control loop has already been established and it was shown that the required accuracy is reachable in the static case [23]. This control loop, however, cannot be directly utilized for the spindle setup, as the position feedback is not continuously available. Thus, the closed loop control has to be adapted accordingly, e.g. using an intermediate thermal expansion model that is parametrized each revolution when the respective segment is measurable.

5. Summary and outlook

In this paper, a novel approach for diamond milling with multiple cutting edges was presented. For achieving the necessary tool setting precision of only a few nanometers, a novel actuating mechanism based on thermal expansion was presented. The design was incorporated into a dedicated tool holder for circumferential milling. By using specifically designed infrared ring lights and control electronics, a selective illumination of the actuating mechanism is possible. Thus, a controllable thermal expansion in radial direction is achieved through a localized heating. The performance of the actuating mechanism was evaluated in static tests and for the first time also on a spindle setup with rotating tool holder. These experiments showed that a thermal expansion of up to $1 \mu\text{m}$ is possible at 240 min^{-1} and thereby confirmed the feasibility of the proposed approach.

Future work will concentrate on further evaluation of the actuator at higher spindle speeds and on regulating the thermal expansion in a closed-loop control.

Acknowledgment

The authors would like to thank the German Research Foundation

(DFG) for funding this work as part of sub-project 1 “Ultra-precise milling with multiple diamond tools” within the research unit FOR 1845 “Ultra-precision High Performance Cutting”.

References

- [1] Dornfeld D, Min S, Takeuchi Y. Recent advances in mechanical micromachining. *CIRP Ann - Manuf Technol* 2006;55(2):745–68. <https://doi.org/10.1016/j.cirp.2006.10.006>.
- [2] Zhang SJ, To S, Zhu ZW, Zhang GQ. A review of fly cutting applied to surface generation in ultra-precision machining. *Int J Mach Tool Manufact* 2016;103:13–27. <https://doi.org/10.1016/j.ijmactools.2016.01.001>.
- [3] Paul E, Evans CJ, Mangamelli A, McGlaufflin ML, Polvani RS. Chemical aspects of tool wear in single point diamond turning. *Precis Eng* 1996;18(1):4–19. [https://doi.org/10.1016/0141-6359\(95\)00019-4](https://doi.org/10.1016/0141-6359(95)00019-4).
- [4] Claylor NE, Combs DM, Lechuga OM, Mader JJ, Udayasankaran J. An overview of freeform optics production. *ASPE winter topical meeting*. 2004.
- [5] Brecher C, Lindemann D, Merz M, Wenzel C, Preuss W. Freeform machining of molds for replication of plastic optics. In: Brinksmeier E, Gläbe R, Riemer O, editors. *Fabrication of complex optical components, lecture notes in production engineering*. Berlin Heidelberg: Springer; 2013. p. 41–52.
- [6] Fang FZ, Zhang XD, Weckenmann A, Zhang G, Evans CJ. Manufacturing and measurement of freeform optics. *CIRP Ann - Manuf Technol* 2013;62(2):823–46. <https://doi.org/10.1016/j.cirp.2013.05.003>.
- [7] Bruzzone AAG, Costa HL, Lonardo PM, Lucca DA. Advances in engineered surfaces for functional performance. *CIRP Ann - Manuf Technol* 2008;57(2):750–69. <https://doi.org/10.1016/j.cirp.2008.09.003>.
- [8] Dutterer BS, Lineberger JL, Smilie PJ, Hildebrand DS, Harriman TA, Davies MA, Suleski TJ, Lucca DA. Diamond milling of an alvarez lens in germanium. *Precis Eng* 2014;38(2):398–408. <https://doi.org/10.1016/j.precisioneng.2013.12.006>.
- [9] Wu Y, Peng W, Liu Y. A novel fabrication method for micro optical waveguide mold based on fly-cutting technology. *Optik Int. J. Light Electron Optic*. 2013;124(9):867–9. <https://doi.org/10.1016/j.ijleo.2012.02.020>.
- [10] Fang FZ, Liu YC. On minimum exit-burr in micro cutting. *J Micromech Microeng* 2004;14(7):984. <http://stacks.iop.org/0960-1317/14/i=7/a=020>.
- [11] Brinksmeier E, Preuss W. Micro-machining. *Phil. Trans. Roy. Soc. A* 2012;370:3973–92. <https://doi.org/10.1098/rsta.2011.0056>.
- [12] Wang SJ, To S, Chen X, Chen XD, Ouyang XB. An integrated optimization of cutting parameters and tool path generation in ultraprecision raster milling. *Int J Adv Manuf Technol* 2014;75(9–12):1711–21. <https://doi.org/10.1007/s00170-014-6254-0>.
- [13] Davies MA, Dutterer BS, Suleski TJ, Silny JF, Kim ED. Diamond machining of diffraction gratings for imaging spectrometers. *Precis Eng* 2012;36(2):334–8. <https://doi.org/10.1016/j.precisioneng.2011.09.006>.
- [14] Schulz H, Moriwaki T. High-speed machining. *CIRP Ann - Manuf Technol* 1992;41(2):637–43. [https://doi.org/10.1016/S0007-8506\(07\)63250-8](https://doi.org/10.1016/S0007-8506(07)63250-8).
- [15] Tlustý J. High-speed machining. *CIRP Ann - Manuf Technol* 1993;42(2):733–8. [https://doi.org/10.1016/S0007-8506\(07\)62536-0](https://doi.org/10.1016/S0007-8506(07)62536-0).
- [16] Solon T. Fundamentals of ultraprecision machining. 2012. p. 56–9. *MachineDesign.com* May 10, 2012 <http://www.precitech.com/downloads/Machine-Design-Article-5-10-12.pdf>.
- [17] Dupont R. Robust rotor dynamics for high-speed air bearing spindles. *Precis Eng* 2015;40:7–13. <https://doi.org/10.1016/j.precisioneng.2014.12.008>.
- [18] Levicron GmbH. Corporate website. 2017 <http://levicron.com>.
- [19] Cheng MN, Cheung CF, Lee WB, To S, Kong LB. Theoretical and experimental analysis of nano-surface generation in ultra-precision raster milling. *Int J Mach Tool Manufact* 2008;48(10):1090–102. <https://doi.org/10.1016/j.ijmactools.2008.02.006>.
- [20] Kong LB, Cheung CF, To S, Lee WB. An investigation into surface generation in ultra-precision raster milling. *J Mater Process Technol* 2009;209(8):4178–85. <https://doi.org/10.1016/j.jmatprotec.2008.11.002>.
- [21] Franco P, Estrems M, Faura F. Influence of radial and axial runouts on surface roughness in face milling with round insert cutting tools. *Int J Mach Tool Manufact* 2004;44(15):1555–65. <https://doi.org/10.1016/j.ijmactools.2004.06.007>.
- [22] Schönemann L, Brinksmeier E, Osmer J. A piezo-driven adaptive tool holder for ultraprecision diamond tool alignment. van Brussel H, Brinksmeier E, Spaan H, Burke T, editors. *9th euspen international conference*, vol. 1. 2009. p. 398–401.
- [23] Schönemann L, Riemer O, Brinksmeier E. Control of a thermal actuator for up-milling with multiple cutting edges. Wertheim R, Ihlefeldt S, Hochmuth C, Putz M, editors. *Procedia CIRP*, vol. 46. 2016. p. 424–7. <https://doi.org/10.1016/j.procir.2016.03.194>.
- [24] Schönemann L, Mejia P, Riemer O, Brinksmeier E. Design and evaluation of a thermal actuator for ultra-precision machining. In: Blunt L, editor. *LAMDAMAP 2015*, euspen, Bedfordshire. 2015. p. 320–30.
- [25] Schönemann L, Riemer O, Brinksmeier E. Using controlled thermal expansion for tool alignment in ultra-precision milling. 30th ASPE annual meeting. 2015. p. 91–4.
- [26] Foremny E, Schenck C, Kuhfuss B. Coupling system for ultra precision machining. *J Mech Eng Autom* 2016;6(6):301–6. <https://doi.org/10.17265/2159-5275/2016.06.006>.